Published in final edited form as:

Arterioscler Thromb Vasc Biol. 2018 February ; 38(2): 353–362. doi:10.1161/ATVBAHA.117.309571.

Growth Differentiation Factor 6 (GDF6) promotes vascular stability by restraining VEGF signaling

Shlomo Krispin[a,I], **Amber N. Stratman**[a,I], **Chase H. Melick**[a], **Radu V. Stan**[b], **Matteo Malinverno**[c], **Jamie Gleklen**[a], **Daniel Castranova**[a], **Elisabetta Dejana**[c,d], and **Brant M. Weinstein**[a,II]

[a]Division of Developmental Biology, *Eunice Kennedy Shriver* National Institute of Child Health and Human Development, NIH, Bethesda, MD, 20892

[b]Departments of Biochemistry and Cell Biology and of Pathology, Geisel School of Medicine at Dartmouth College, Lebanon, NH 03756

[c]Vascular Biology Program, IFOM, FIRC Institute of Molecular Oncology Foundation, Milan, Italy

[d]Department of Immunology, Genetics and Pathology, Uppsala University, Sweden

Abstract

Objective—The assembly of a functional vascular system requires a coordinated and dynamic transition from activation to maturation. High VEGF activity promotes activation, including junction destabilization and cell motility. Maturation involves junctional stabilization and formation of a functional endothelial barrier. The identity and mechanism of action of pro-stabilization signals is still mostly unknown. Bone morphogenetic protein (BMP) receptors and their ligands have important functions during embryonic vessel assembly and maturation. Previous work has suggested a role for GDF6 (BMP13) in vascular integrity, although GDF6's mechanism of action was not clear. Therefore, we sought to further explore the requirement for GDF6 in vascular stabilization.

Approach and Results—We investigated the role of GDF6 in promoting endothelial vascular integrity *in vivo* in zebrafish and in cultured Human Umbilical Vein Endothelial Cells (HUVEC) *in vitro*. We report that GDF6 promotes vascular integrity by counteracting VEGF activity. GDF6-deficient endothelium has increased VEGF signaling, increased VE-cadherin Y658 phosphorylation, VE-cadherin delocalization from cell-cell interfaces, and weakened endothelial cell adherence junctions that become prone to vascular leak.

Conclusions—Our results suggest that GDF6 promotes vascular stabilization by restraining VEGF signaling. Understanding how GDF6 affects vascular integrity may help to provide insights into hemorrhage and associated vascular pathologies in humans.

[II]Corresponding Author: Brant M. Weinstein, Associate Scientific Director, Division of Developmental Biology, *Eunice Kennedy Shriver* National Institute of Child Health and Human Development, Building 6B, Room 413, 6 Center Drive, Bethesda, MD, 20892. flyingfish2@nih.gov.

[I]These authors contributed equally.

Disclosures – None

Keywords

Growth Differentiation Factor 6; GDF6; VEGF; VE-Cadherin; VECDN

INTRODUCTION

The complex body design of vertebrates requires efficient transport of gases, liquids, nutrients and circulating cells between tissues and organs. This task is carried out by the highly branched cardiovascular system. Endothelial cells line the lumen of blood vessels and form a semipermeable monolayer that controls blood-tissue fluid and nutrient exchange. The integrity of the endothelial barrier is essential for physiological tissue homeostasis, and hyperpermeability is involved in the progression of several pathological conditions, including inflammation, atherosclerosis, and cancer (1). During development, the vascular network is formed mainly by angiogenesis – the formation of new blood vessels from preexisting ones. In conditions that favor angiogenesis, some endothelial cells respond to Vascular Endothelial Growth Factor (VEGF) cues by loosening their connections with neighboring cells and becoming invasive and migratory (2). The zebrafish embryo provides a useful model system for studying these complex cellular behaviors, as it enables visualization of the vascular network *in vivo* in a developing embryo. As we have described previously (3), intersegmental vessels (ISVs) emerge from the dorsal aorta (DA) starting at approximately 20 hpf, migrating dorsally along the somite boundaries in response to VEGF and other cues. At 32 hpf, roughly 12 hrs after initial ISV sprouting, ISV tip cells approach each other to fuse and form the dorsal longitudinal anastomotic vessel (DLAV). Over the course of the following 18 hrs the system stabilizes, forming continuous lumens throughout and greatly reducing EC protrusive activity. This maturation phase may be controlled by pro-stabilization signals that counteract VEGF activity, leading to adherence junction stabilization and formation of functional barrier. However, the identity and mechanism of action of pro-stabilization signals is still unknown.

A variety of genetic and experimental data suggest that bone morphogenetic protein (BMP) signaling has a crucial role in maintaining vascular integrity (4–7). GDF6 (BMP13) is a BMP family member belonging to the Growth Differentiation Factor subgroup. The amino acid sequence for GDF6 (BMP13) is highly conserved across vertebrates, with sequence homology concentrated in the active C-terminal domain. Even the most divergent of BMP13-homologues, Zebrafish *gdf6a* (radar) and *gdf6b* (dynamo), display greater than 90% homology in this domain (8). The role of GDF6 is probably best understood in regulating bone and ocular development across a number of species, including humans. Patients with mutations in the GDF6 gene, such as those noted in Klippel-Feil syndrome, can phenotypically present with fusion of the vertebrae and limited mobility in addition to having a number of ocular disorders (9, 10). Ocular disorders known to be linked to mutations in GDF6 include microphthalmia, coloboma, and age-related macular degeneration (AMD) (11–15). An AMD “risk allele” linked to GDF6 is also associated with increased expression of HTRA1, and HTRA1 knockout mice show decreased vascular development in the retina together with increased GDF6 and decreased VEGFA expression (15).A previous report using morpholino knockdown suggested a role for *gdf6a* in

establishment of trunk vasculature integrity in the zebrafish (16). However, the precise mechanism by which *gdf6a* regulates vascular integrity is unclear and is the focus of this study.

Adherence junctions (AJs), and the key AJ component VE-cadherin in particular play an important role in the control of vascular permeability and integrity (17, 18). Barrier-destabilizing agents such as VEGF can induce increases in vascular permeability through modulation of the activity of different small GTPases. VEGF stimulation of endothelial cells activates Src, which stimulates Vav2, Rac1, and its downstream effector PAK1. In turn, PAK1 phosphorylates a serine residue (Ser665) in the cytoplasmic tail of VE-cadherin, thereby promoting its endocytosis and increasing the vascular permeability (19). More recently, c-Src–dependent phosphorylation of VE-cadherin at Tyr658 was found to induce uncoupling of p120-catenin from VE-cadherin, resulting in internalization of VE-cadherin from AJs and subsequent loss of endothelial barrier function (20).

In this study, we report a previously uncharacterized trunk hemorrhage phenotype in *gdf6a*^{s327} zebrafish mutants and examine the consequences of GDF6 loss of function for endothelial cells *in vivo* and *in vitro*. We find that GDF6 is required for proper endothelial barrier function, and that it acts as a negative regulator of VEGFR2 receptor levels and VEGF signaling. In addition to increased receptor levels, GDF6-deficient endothelial cells show increased downstream ERK activation and increased phosphorylation, destabilization, and internalization of VE-cadherin. Together, our results suggest that GDF6 function promotes vascular quiescence and endothelial barrier function by restraining VEGF signaling-dependent junction destabilization.

MATERIALS AND METHODS

Materials and methods are available in the on-line only data supplement.

RESULTS

GDF6 loss of function results in impaired vascular structural integrity and increased vascular permeability

Zebrafish have two GDF6 orthologs, *gdf6a* and *gdf6b*. However, whole mount *in situ* hybridization reveals that *gdf6a* is the sole GDF6 player expressed in the zebrafish trunk at 48 hpf (Figure 1A–C), so we focused on this gene for our analysis. At 48 hpf *gdf6a* is expressed in endothelial cells of the axial vasculature (DA and PCV) and in the dorsal fin fold adjacent to the newly formed DLAV (Figure 1B). To investigate the role of *gdf6a* in vascular integrity, we examined zebrafish carrying the *gdf6a*^{s327} mutation. This mutation results in a single C to A substitution in position 164 of the *gdf6a* coding sequence, introducing a stop codon early in the *gdf6a* open reading frame (13). The mutant allele is predicted to encode a truncated pro-protein of 54 amino acids lacking the putative C-terminal mature signal peptide. As previously reported, mutants develop on a comparable schedule compared to their WT siblings (Figure 1D,E) but they display microphthalmia and melanocyte mispatterning (Figure 1F,G). Additionally, we find that 25% of *gdf6a*^{s327} mutants also develop trunk hemorrhage (Figure 1G–N). The hemorrhages gradually clear

over the next two days of development, and 90% of hemorrhaging mutants are homozygous viable. The hemorrhage phenotype could be phenocopied by *gdf6a* morpholino knock down, with 24% of embryos injected with 5 ng of gdf6a 5' splice blocking morpholino developing trunk hemorrhage at 48 hpf (Figure 1O,P).

To better understand the effects of loss of *gdf6a* on trunk endothelial barrier function we analyzed vascular patterning and stability in gdf6a mutants. In severe cases of massive hemorrhage we found evidence for impaired vascular structural integrity around the lesion site (Figure 1I–N). However, in non-hemorrhaging mutants or mutants with very small hemorrhages the pattern and morphology of trunk vessels did not appear significantly affected, suggesting vessel malformation is not a primary defect in *gdf6a*^{s327} mutants. Additionally, vascular outgrowth and intersegmental vessel formation appear normal prior to the onset of the hemorrhage phenotype (Figure 1D,E). To further examine vascular barrier function and vascular integrity in *gdf6a*^{s327} mutants, we injected 20 nm Qdot 655 fluorescent nanocrystals into the circulation of non-hemorrhaging 48hpf mutants (as assessed by their fully penetrant micropthalmia phenotype) or their phenotypically wild type siblings. We found that 73% of injected non-hemorrhaging mutants showed focal leakage of the Qdot655 nanocrystals, despite the fact that none of these animals displayed hemorrhage (Figure 1Q–W). These results suggest that vascular barrier dysfunction is present in a large majority of *gdf6a*^{s327} mutants despite the fact that obvious large-scale vascular rupture (hemorrhage) occurs in only 25% of mutants.

To further support the idea that the effects on vascular barrier function in *gdf6a*^{s327} mutants are a direct consequence of loss of *gdf6a*, we used inducible expression of wild type *gdf6a* to rescue the hemorrhage phenotype in mutants. Since *gdf6a* is maternally deposited and plays a crucial role in early dorsal-ventral patterning (21), we used heat shock-inducible expression of *gdf6a-2a-mcherry* transgene with induction starting at 32 hpf in order to avoid effects on early embryonic patterning. The hemorrhage phenotype was rescued by heat-shock inducible *gdf6a* expression, with the frequency of hemorrhage dropping from 33% in control *mcherry* transgene-injected *gdf6a*^{s327} embryos to 8% in *gdf6a-2a-mcherry* transgene-injected animals (Figure 1X).

GDF6 expression is also present in human endothelial cells including Human Umbilical Vein Endothelial Cells (HUVEC), as revealed by RT-PCR analysis. To test whether the role of GDF6 in promoting endothelial barrier function is evolutionarily conserved, we knocked down GDF6 in HUVEC cells using siRNA (Figure 2A,B) and then subjected GDF6 or control siRNA-treated HUVEC to a transwell dye leakage vascular permeability assay (Figure 2C). Assembly of an endothelial monolayer from control siRNA-treated HUVEC ("Control siRNA") reduced transwell permeability to less than 20% of that present in the absence of cells ("No Cell Control"), while assembly of an endothelial monolayer from GDF6 siRNA-treated HUVEC ("GDF6 siRNA") resulted in a 2.5 fold increase in transwell permeability compared to the control siRNA-treated cell monolayer (to 50% of the "No Cell Control"; Figure 2D). The increased permeability noted in GDF6 siRNA conditions could be largely or completely reversed by either administration of recombinant GDF6 protein or depletion of VEGFA ligand from the assay using an anti-VEGFA neutralizing antibody (Figure 2D). As positive and negative controls for this assay, addition of recombinant

VEGFA protein or sphingosine-1-phosphate (S1P) to HUVEC monolayers resulted in increased or decreased permeability, respectively (Figure 2E). These results support a crucial role for GDF6 as a pro-stabilization cue and a potential role for GDF6/VEGF signaling in regulation of endothelial cell-cell junctions.

GDF6 loss of function results in increased VEGF signaling in endothelial cells

Our results show that loss of GDF6 results in endothelial barrier dysfunction but that removal of VEGFA from the system can rescue this phenotype (Figure 2D). We hypothesize that GDF6 might stabilize the developing vasculature by counteracting the effects of VEGF signaling, with loss of GDF6 resulting in a disregulated angiogenic balance “tipped” toward the activation state. VEGF signals through VEGFR2 to activate endothelial cells. Activation of VEGFR2 results in phosphorylation of several residues in the VEGFR2 cytoplasmic tail (22), including Tyr1175, whose phosphorylation leads to ERK activation that in turn increases cell motility and decreases stability (Figure 3A) (23, 24). We examined the levels of total and Tyr1175 phosphorylated VEGFR2 protein in control or GDF6 siRNA-treated HUVEC using western blotting, and found that GDF6 knockdown results in an approximately two-fold increase in both Tyr1175 phosphorylated and total levels of VEGFR2 (Figure 3B,C). The proportional increase in total- and phospho-VEGFR2 levels suggests that the increase in Tyr1175 phosphorylated VEGFR2 can be attributed mainly to an increase in the total receptor levels. The increase in total VEGFR2 protein levels could be partially rescued by the readministration of recombinant GDF6 protein to the HUVEC growth media (Figure 3D). Next, we quantified VEGFR2 mRNA transcript levels in control or GDF6 siRNA-treated HUVEC by quantitative RT-PCR analysis. We found that that GDF6 knockdown in HUVECs results in an approximately three and a half-fold increase in VEGFR2 transcript levels (Figure 3E). Total VEGFR2 transcript levels are also increased in *gdf6a*^{s327} mutants *in vivo* as assessed by both quantitative RT-PCR (Figure 3F) and by whole mount *in situ* hybridization (Figure 3G,H), although not to as great an extent as in knockdown HUVEC *in vitro*. Together, these results suggest that loss of GDF6 function results in increased expression and accumulation of VEGFR2 receptor.

To examine whether signaling downstream from the VEGFR2 receptor was also increased, we examined the phosphorylation of ERK1/2. As noted above, VEGFR2 receptor phosphorylation triggers phosphorylation or ERK, which in turn promotes increased endothelial motility and decreased stability (Figure 3A). We examined the levels of both total and Thr202/Tyr205-phosphorylated (25) ERK1/2 protein in control or GDF6 siRNA-treated HUVEC using western blotting, and found that GDF6 knockdown results in an approximately 1.6-fold increase in phospho-ERK1/2 without altering total protein levels (Figure 4A,B). Measurement of endothelial phospho-ERK was also carried out in in *gdf6a*^{s327} mutants by quantifying ERK activation in the trunk axial vessels of phospho-ERK1/2 immunostained mutants versus their wild type siblings (Figure 4C–G, showing a 2.3-fold increase in phospho-ERK1/2 in *gdf6a*^{s327} mutants. Together, these results suggest that GDF6 functions to restrain VEGFR2 levels and VEGF signaling.

GDF6 loss of function results in defective endothelial cell-cell junction formation

Elevated VEGF signaling is associated with increased permeability and decreased barrier function in the endothelium – indeed, VEGF was originally identified as "Vascular Permeability Factor" (VPF) based on its ability to induce vascular leakage (26). These effects are due in part to both destabilization of endothelial cell-cell junctions and increased trans-endothelial transport (1). VEGF-induced fenestration allows leakage of small solutes, and passage of proteins has been attributed to VEGF-induced formation of caveolae, assembly of caveolae into vesiculovacuolar organelles (VVOs), and/or induction of trans-endothelial pores (27, 28). Leakage of larger proteins and extravasation of red blood cells depend on VE-Cadherin mediated loosening of adherence junctions, which allows passage between endothelial cells (1). We examined the ultrastructure of blood vessels and endothelial cell junctions in *gdf6a*^{s327} mutants and their wild type siblings in order to determine whether mutant endothelium exhibits some of the characteristics noted above.

We performed electron microscopy on transverse sections of the mid-trunk of 48 hpf zebrafish *gdf6a*^{s327} mutant or wild type sibling animals to assess vascular endothelial cell morphology and ultrastructure. The gross morphology of mutants was substantially normal, and both axial vessels (dorsal aorta and cardinal vein) were clearly evident in both wild type and mutant animals. Electron micrographs of the endothelial lining of the dorsal aorta revealed a single endothelial cell layer in either *gdf6a*^{s327} mutant or wild type sibling animals (Figure 5A–H). In wild type siblings, endothelial cell-cell junctions were clearly visible on the dorsal aorta (Figure 5A–D). These wild type junctions generally showed closely apposed cell membranes with numerous electron-dense areas on and near cell-cell interfaces (red arrows in Figure 5B,D). Endothelial cell-cell junctions were also readily visualized on the dorsal aorta in *gdf6a*^{s327} mutants, but they often appeared less well developed, displaying less closely apposed membranes and fewer junctional electron-dense areas (Figure 5E–H). Quantitative measurement of the average length of dorsal aorta junctions in *gdf6a*^{s327} mutants compared to their wild type siblings showed that junctions are on average substantially shorter in mutants than in wild type animals (Figure 5I). *gdf6* loss of function has been linked to an increase in apoptosis of tissue in the developing eye (14). To rule out increased cell death, Caspase 3 staining was carried out on *gdf6a*^{s327} mutants and their wild type siblings, revealing no increase in the number of apoptotic ECs in the dorsal aorta prior to the onset of hemorrhage (Figure 5J–M). Together, these results confirm that failure to counteract VEGF signaling with GDF6 leads to ultrastructurally apparent defects in endothelial cell-cell junctions without an apparent increase in EC death.

GDF6 loss of function results in increased VE-Cadherin internalization and degradation

Adherence junctions (AJs), and the AJ key component VE-Cadherin (VECDN) in particular, play an important role in the control of vascular permeability and integrity (17, 18, 29). As noted above, VEGF is a well-known permeability-inducing agent. VEGF activation is known to initiate an intracellular cascade of events that leads to phosphorylation of VECDN on Tyrosine 658, promoting VECDN internalization and degradation, ultimately increasing trans-endothelial permeability (Figure 6A; (20, 30, 31)). To test whether *in vivo* loss of GDF6 results in VE-cadherin destabilization, we began by using western blotting to examine the total levels of VECDN protein in hemorrhaging or non-hemorrhaging zebrafish

gdf6a^{s327} mutants, compared to their wild-type siblings (Figure 6B,C). We found that *gdf6a*^{s327} mutants have 35–40% less VECDN protein than wild type siblings, with similar VECDN protein levels in *gdf6a*^{s327} mutants with and without visible hemorrhage. We also examined levels of both total and phospho-VECDN (Tyr658) in control and GDF6 siRNA-treated HUVEC *in vitro* by western blotting (Figure 6D,E). Although GDF6 loss of function in HUVEC did not lead to significant reduction in levels of total VECDN, phospho-VECDN levels were substantially increased, suggesting that VECDN is being destabilized in GDF6-deficient endothelial cells. To further examine the role of GDF6 in endothelial junction formation, we use immunofluorescence to examine PECAM, total VECDN, and phospho-VECDN localization in control or GDF6 siRNA-treated HUVEC forming an endothelial monolayer in culture. GDF6-deficient HUVEC showed reduced PECAM and VECDN localization at endothelial cell-cell interfaces but strong phospho-VECDN staining of residual junctions (Figure 6F–O), confirming that junction disassembly occurs in the absence of GDF6. Treatment of control HUVECs with VEGFA ligand or S1P were used as positive and negative controls for junctional assembly. Treatment with VEGFA resulted in decreased VECDN localization at endothelial cell-cell interfaces and high levels of phospho-VECDN staining of residual junctions, while treatment with S1P showed the opposite effects (Figure 6P–U).

DISCUSSION

Together, our results suggest that GDF6 functions to antagonize VEGF mediated phosphorylation of VECDN by reducing VEGFR2 receptor levels, preventing destabilization, internalization, and degradation of VECDN and promoting junctional stability and vascular integrity (Figure 6V). In line with these observations, we showed recently that partial reduction of zebrafish VECDN expression using low doses of morpholinos causes vascular fragility, hemorrhage, and increased trunk vessel permeability (32). Interestingly, VECDN also appears to alter TGF-β signaling in the endothelium, with VECDN regulating VEGF/ERK1/2 and TGF-β/Smad signaling pathways in opposite ways with identical biological outcomes in endothelial cells (33). The formation of a VECDN–VEGFR2 complex limits cell proliferation by preventing ERK1/2 activation (34), while formation of VECDN-TGF-β receptor complexes promotes TGF-β-induced Smad2/3 phosphorylation leading to vascular stabilization (33). A “pro-quiescence” role has also been described for other BMP superfamily members, including BMP9 and BMP10. BMP type II receptor (BMPR2) was found to form a signaling complex with activin receptor-like kinase 1 (ALK1/ACTVRL1) and signal specifically in response to BMP9/10 in microvascular endothelial cells (35). Unlike other BMPs, BMP9 circulates at measureable concentrations in serum and is thought to act as a vascular quiescence factor, blocking angiogenesis *in vitro* (36) and *in vivo* (35, 37), making it a candidate for therapeutically targeting the dysfunctional pulmonary endothelium in pulmonary arterial hypertension (PHT) patients (38). Mutations in BMPR2 and ALK1 are associated with PHT (39, 40). Moreover, Li and colleagues showed that in adult mice, stably silencing BMPR2 expression by RNA interference results in severe mucosal hemorrhage and incomplete mural cell coverage of vessel walls (7). Interestingly, pulmonary artery EC (PAEC) from Bmpr2(+/−) mice have a constitutively active SRC kinase, an increased number of caveolae, and impaired endothelial

barrier function (41). Our results suggest that the cause of some of these phenotypes may be misregulated VEGF signaling activity rather than action on direct downstream targets of BMP signaling. The involvement of additional signaling pathways in the pathophysiology of BMP-related vascular diseases would open new therapeutic horizons for these disorders.

The link between GDF6 and modulation of the VEGF receptor still remains to be determined. The specific receptors transducing GDF6 activity are still unclear, although GDF6 has a demonstrated preferential affinity for BMPR1B (ALK6) and BMPR2 (42). In a rat osteoblast cell line (ROB-C26), GDF6 forms complexes with BMPR1B and BMPR2 to transduce a strong transcription initiation signal, as measured by the use of a luciferase reporter gene with the 3TP promoter that contains three consecutive TPA response elements (TREs) and a portion of the plasminogen activator inhibitor 1 (PAI-1) promoter region. A weaker signal and barely detectable receptor complex is associated with BMPR1A (ALK3)/ BMPR2 (Erlacher et al., 1998). The receptors and downstream signaling pathways utilized by GDF6 in endothelial cells need to be examined further, however. Together, our results and previous studies on the function of TGFb and BMP family members in the vasculature suggest complex roles in regulating vascular quiescence and maturation.

Supplementary Material

Refer to Web version on PubMed Central for supplementary material.

Acknowledgments

The authors would like to thank Andrew Waskiewicz for providing the *gdf6a*^{s327} mutant line. The authors would also like to thank members of the Weinstein laboratory for their critical comments on this manuscript.

Sources of Funding -

This work was supported by the intramural program of the Eunice Kennedy Shriver National Institute of Child Health and Human Development, National Institutes of Health (ZIA HD008915, to BMW), by the National Institutes of Health (GM120592, CA172983 and CA175592 to RVS), by the American Heart Association (16GRNT27260362 to RVS), by the Knut and Alice Wallemberg Foundation (to ED), and by an NIH K99 Pathway to Independence Award (NHLBI/NIH, to ANS).

ABBREVIATIONS

BMP13	Bone Morphogenetic Protein 13 (aka GDF6)
BMPR2	Bone Morphogenetic Protein Receptor 2
DA	Dorsal Aorta
DLAV	dorsal longitudinal anastomotic vessel
GDF6	Growth Differentiatin Factor 6
ISV	Intersegmental Vessels
siRNA	Small Interfering Ribonucleic Acid
PCV	Posterior Cardinal Vein

PHT	pulmonary arterial hypertension
TGFβ	Transforming Growth Factor Beta
VECDN	Vascular Endothelial Cadherin (aka Cadherin 5)
VEGF	Vascular Endothelial Growth Factor
VEGFR2	Vascular Endothelial Growth Factor Receptor 2 (aka Flk1).

References

1. Weis SM, Cheresh DA. Pathophysiological consequences of VEGF-induced vascular permeability. Nature. 2005; 437:497–504. [PubMed: 16177780]
2. Adams RH, Alitalo K. Molecular regulation of angiogenesis and lymphangiogenesis. Nat Rev Mol Cell Biol. 2007; 8:464–478. [PubMed: 17522591]
3. Isogai S, Lawson ND, Torrealday S, Horiguchi M, Weinstein BM. Angiogenic network formation in the developing vertebrate trunk. Development. 2003; 130:5281–5290. [PubMed: 12954720]
4. Cai J, Pardali E, Sanchez-Duffhues G, ten Dijke P. BMP signaling in vascular diseases. FEBS Lett. 2012; 586:1993–2002. [PubMed: 22710160]
5. de Vinuesa AG, Bocci M, Pietras K, Ten Dijke P. Targeting tumour vasculature by inhibiting activin receptor-like kinase (ALK)1 function. Biochem Soc Trans. 2016; 44:1142–1149. [PubMed: 27528762]
6. Itoh F, Itoh S, Adachi T, Ichikawa K, Matsumura Y, Takagi T, et al. Smad2/Smad3 in endothelium is indispensable for vascular stability via S1PR1 and N-cadherin expressions. Blood. 2012; 119:5320–5328. [PubMed: 22498737]
7. Liu D, Wang J, Kinzel B, Mueller M, Mao X, Valdez R, et al. Dosage-dependent requirement of BMP type II receptor for maintenance of vascular integrity. Blood. 2007; 110:1502–1510. [PubMed: 17496203]
8. Williams LA, Bhargav D, Diwan AD. Unveiling the bmp13 enigma: redundant morphogen or crucial regulator? Int J Biol Sci. 2008; 4:318–329. [PubMed: 18797508]
9. Asai-Coakwell M, French CR, Ye M, Garcha K, Bigot K, Perera AG, et al. Incomplete penetrance and phenotypic variability characterize Gdf6-attributable oculo-skeletal phenotypes. Hum Mol Genet. 2009; 18:1110–1121. [PubMed: 19129173]
10. Tassabehji M, Fang ZM, Hilton EN, McGaughran J, Zhao Z, de Bock CE, et al. Mutations in GDF6 are associated with vertebral segmentation defects in Klippel-Feil syndrome. Hum Mutat. 2008; 29:1017–1027. [PubMed: 18425797]
11. Asai-Coakwell M, French CR, Berry KM, Ye M, Koss R, Somerville M, et al. GDF6, a novel locus for a spectrum of ocular developmental anomalies. Am J Hum Genet. 2007; 80:306–315. [PubMed: 17236135]
12. den Hollander AI, Biyanwila J, Kovach P, Bardakjian T, Traboulsi EI, Ragge NK, et al. Genetic defects of GDF6 in the zebrafish out of sight mutant and in human eye developmental anomalies. BMC Genet. 2010; 11:102. [PubMed: 21070663]
13. Gosse NJ, Baier H. An essential role for Radar (Gdf6a) in inducing dorsal fate in the zebrafish retina. Proc Natl Acad Sci U S A. 2009; 106:2236–2241. [PubMed: 19164594]
14. Pant SD, March LD, Famulski JK, French CR, Lehmann OJ, Waskiewicz AJ. Molecular mechanisms regulating ocular apoptosis in zebrafish gdf6a mutants. Invest Ophthalmol Vis Sci. 2013; 54:5871–5879. [PubMed: 23847306]
15. Zhang L, Lim SL, Du H, Zhang M, Kozak I, Hannum G, et al. High temperature requirement factor A1 (HTRA1) gene regulates angiogenesis through transforming growth factor-beta family member growth differentiation factor 6. J Biol Chem. 2012; 287:1520–1526. [PubMed: 22049084]
16. Hall CJ, Flores MV, Davidson AJ, Crosier KE, Crosier PS. Radar is required for the establishment of vascular integrity in the zebrafish. Dev Biol. 2002; 251:105–117. [PubMed: 12413901]

17. Giannotta M, Trani M, Dejana E. VE-cadherin and endothelial adherens junctions: active guardians of vascular integrity. Dev Cell. 2013; 26:441–454. [PubMed: 24044891]
18. Dejana E, Tournier-Lasserve E, Weinstein BM. The control of vascular integrity by endothelial cell junctions: molecular basis and pathological implications. Dev Cell. 2009; 16:209–221. [PubMed: 19217423]
19. Gavard J, Gutkind JS. VEGF controls endothelial-cell permeability by promoting the beta-arrestin-dependent endocytosis of VE-cadherin. Nat Cell Biol. 2006; 8:1223–1234. [PubMed: 17060906]
20. Hatanaka K, Simons M, Murakami M. Phosphorylation of VE-cadherin controls endothelial phenotypes via p120-catenin coupling and Rac1 activation. Am J Physiol Heart Circ Physiol. 2011; 300:H162–172. [PubMed: 21037229]
21. Sidi S, Goutel C, Peyrieras N, Rosa FM. Maternal induction of ventral fate by zebrafish radar. Proc Natl Acad Sci U S A. 2003; 100:3315–3320. [PubMed: 12601179]
22. Olsson AK, Dimberg A, Kreuger J, Claesson-Welsh L. VEGF receptor signalling - in control of vascular function. Nat Rev Mol Cell Biol. 2006; 7:359–371. [PubMed: 16633338]
23. Takahashi T, Yamaguchi S, Chida K, Shibuya M. A single autophosphorylation site on KDR/Flk-1 is essential for VEGF-A-dependent activation of PLC-gamma and DNA synthesis in vascular endothelial cells. EMBO J. 2001; 20:2768–2778. [PubMed: 11387210]
24. Holmqvist K, Cross MJ, Rolny C, Hagerkvist R, Rahimi N, Matsumoto T, et al. The adaptor protein shb binds to tyrosine 1175 in vascular endothelial growth factor (VEGF) receptor-2 and regulates VEGF-dependent cellular migration. J Biol Chem. 2004; 279:22267–22275. [PubMed: 15026417]
25. Lamalice L, Le Boeuf F, Huot J. Endothelial cell migration during angiogenesis. Circ Res. 2007; 100:782–794. [PubMed: 17395884]
26. Senger DR, Galli SJ, Dvorak AM, Perruzzi CA, Harvey VS, Dvorak HF. Tumor cells secrete a vascular permeability factor that promotes accumulation of ascites fluid. Science. 1983; 219:983–985. [PubMed: 6823562]
27. Dvorak HF, Nagy JA, Feng D, Brown LF, Dvorak AM. Vascular permeability factor/vascular endothelial growth factor and the significance of microvascular hyperpermeability in angiogenesis. Curr Top Microbiol Immunol. 1999; 237:97–132. [PubMed: 9893348]
28. Baluk P, Fuxe J, Hashizume H, Romano T, Lashnits E, Butz S, et al. Functionally specialized junctions between endothelial cells of lymphatic vessels. J Exp Med. 2007; 204:2349–2362. [PubMed: 17846148]
29. Dejana E, Orsenigo F. Endothelial adherens junctions at a glance. J Cell Sci. 2013; 126:2545–2549. [PubMed: 23781019]
30. Wallez Y, Cand F, Cruzalegui F, Wernstedt C, Souchelnytskyi S, Vilgrain I, et al. Src kinase phosphorylates vascular endothelial-cadherin in response to vascular endothelial growth factor: identification of tyrosine 685 as the unique target site. Oncogene. 2007; 26:1067–1077. [PubMed: 16909109]
31. Orsenigo F, Giampietro C, Ferrari A, Corada M, Galaup A, Sigismund S, et al. Phosphorylation of VE-cadherin is modulated by haemodynamic forces and contributes to the regulation of vascular permeability in vivo. Nat Commun. 2012; 3:1208. [PubMed: 23169049]
32. Montero-Balaguer M, Swirsding K, Orsenigo F, Cotelli F, Mione M, Dejana E. Stable vascular connections and remodeling require full expression of VE-cadherin in zebrafish embryos. PLoS One. 2009; 4:e5772. [PubMed: 19503615]
33. Rudini N, Felici A, Giampietro C, Lampugnani M, Corada M, Swirsding K, et al. VE-cadherin is a critical endothelial regulator of TGF-beta signalling. EMBO J. 2008; 27:993–1004. [PubMed: 18337748]
34. Lampugnani MG, Orsenigo F, Gagliani MC, Tacchetti C, Dejana E. Vascular endothelial cadherin controls VEGFR-2 internalization and signaling from intracellular compartments. J Cell Biol. 2006; 174:593–604. [PubMed: 16893970]
35. David L, Mallet C, Vailhe B, Lamouille S, Feige JJ, Bailly S. Activin receptor-like kinase 1 inhibits human microvascular endothelial cell migration: potential roles for JNK and ERK. J Cell Physiol. 2007; 213:484–489. [PubMed: 17620321]

36. Scharpfenecker M, van Dinther M, Liu Z, van Bezooijen RL, Zhao Q, Pukac L, et al. BMP-9 signals via ALK1 and inhibits bFGF-induced endothelial cell proliferation and VEGF-stimulated angiogenesis. J Cell Sci. 2007; 120:964–972. [PubMed: 17311849]

37. Laux DW, Young S, Donovan JP, Mansfield CJ, Upton PD, Roman BL. Circulating Bmp10 acts through endothelial Alk1 to mediate flow-dependent arterial quiescence. Development. 2013; 140:3403–3412. [PubMed: 23863480]

38. Long L, Ormiston ML, Yang X, Southwood M, Graf S, Machado RD, et al. Selective enhancement of endothelial BMPR-II with BMP9 reverses pulmonary arterial hypertension. Nat Med. 2015; 21:777–785. [PubMed: 26076038]

39. Deng Z, Morse JH, Slager SL, Cuervo N, Moore KJ, Venetos G, et al. Familial primary pulmonary hypertension (gene PPH1) is caused by mutations in the bone morphogenetic protein receptor-II gene. Am J Hum Genet. 2000; 67:737–744. [PubMed: 10903931]

40. Harrison RE, Flanagan JA, Sankelo M, Abdalla SA, Rowell J, Machado RD, et al. Molecular and functional analysis identifies ALK-1 as the predominant cause of pulmonary hypertension related to hereditary haemorrhagic telangiectasia. J Med Genet. 2003; 40:865–871. [PubMed: 14684682]

41. Prewitt AR, Ghose S, Frump AL, Datta A, Austin ED, Kenworthy AK, et al. Heterozygous null bone morphogenetic protein receptor type 2 mutations promote SRC kinase-dependent caveolar trafficking defects and endothelial dysfunction in pulmonary arterial hypertension. J Biol Chem. 2015; 290:960–971. [PubMed: 25411245]

42. Erlacher L, McCartney J, Piek E, ten Dijke P, Yanagishita M, Oppermann H, et al. Cartilage-derived morphogenetic proteins and osteogenic protein-1 differentially regulate osteogenesis. J Bone Miner Res. 1998; 13:383–392. [PubMed: 9525338]

HIGHLIGHTS

- The BMP family ligand GDF6 (BMP13) stabilizes the endothelial wall
- GDF6 promotes vascular integrity by counteracting VEGF activity
- GDF6 suppresses VEGFR2 levels and VE-cadherin Y658 phosphorylation
- GDF6-deficient endothelium has delocalized VE-cadherin and weakened junctions prone to leakage
- This work may provide insights into hemorrhage and associated vascular pathologies in humans.

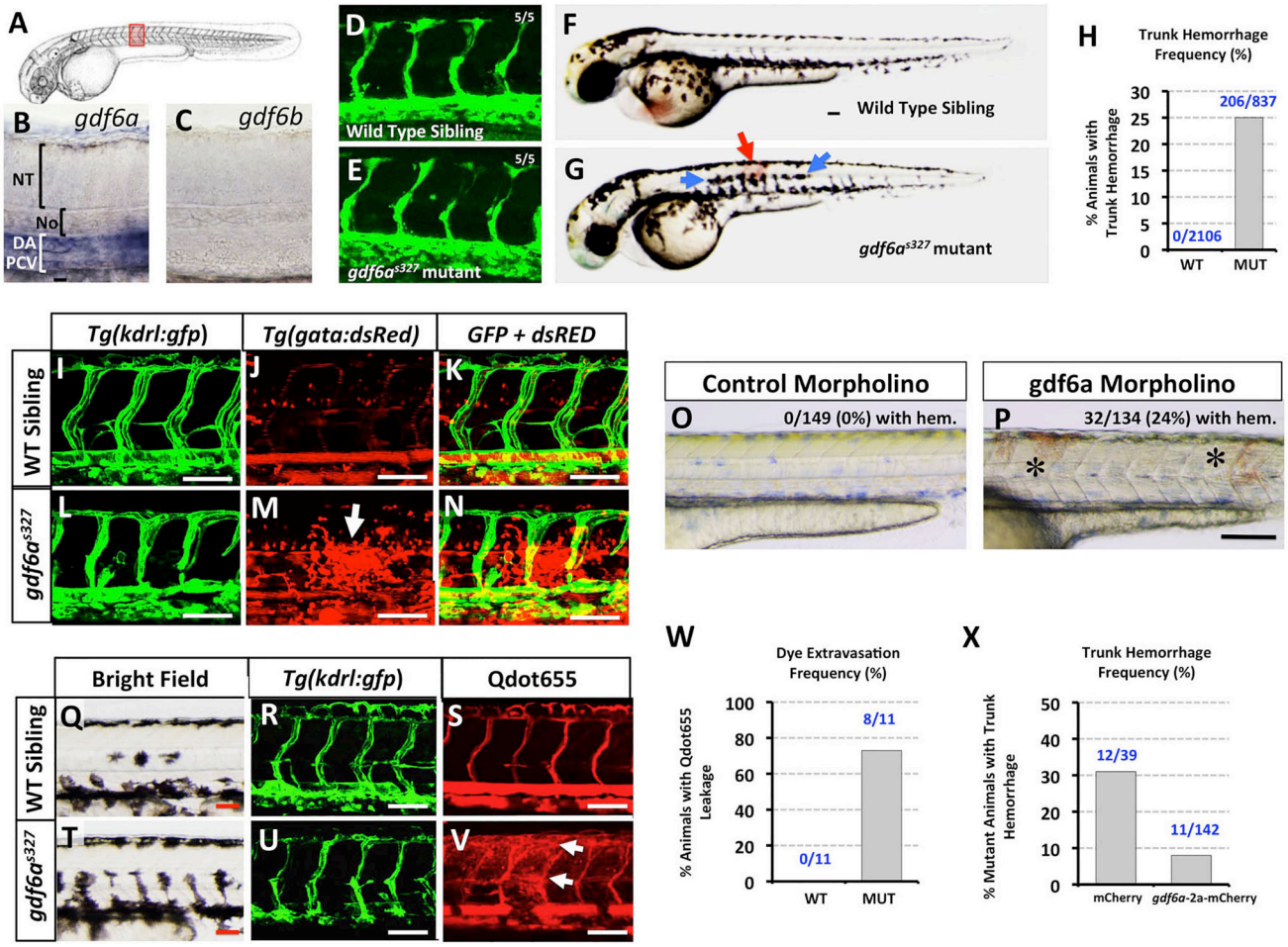

Figure 1. Loss of GDF6 function results in impaired vascular integrity *in vivo*

(**A**) Camera lucida drawing of a 2 dpf zebrafish embryo, with the red box indicating the region imaged in panels B and C. (**B,C**) Whole mount *in situ* hybridization of the mid-trunk of 2 dpf wild-type zebrafish embryos probed for either *gdf6a* (B) or *gdf6b* (C). WM-ISH was performed in 3 biological replicates with at least 10 embryos per experimental group. (**D,E**) Representative confocal images of ~1.5 dpf age mattched wild type (D) versus *gdf6a*^{s327} mutant (E) animals in a *Tg(kdrl:gfp)* background showing normal outgrowth and patterning of the intersegmental vessels. (**F,G**) Transmitted light images of whole 2 dpf wild type sibling (F) or *gdf6a*^{s327} mutant (G) animals, showing small eyes (black arrows), pigment mispatterning (blue arrows), and trunk hemorrhage (red arrow) in the *gdf6a*^{s327} mutant. (**H**) Quantification of the percentage of 2 dpf wild type sibling (0/2106 in 24 separate clutches, 0%) or *gdf6a*^{s327} mutant animals 206/837 in 24 separate clutches, 25%) displaying trunk hemorrhage. (**I–N**) Representative confocal images of a 2 dpf wild type sibling (I–K) or *gdf6a*^{s327} mutant (L–N) *Tg(kdrl:gfp), Tg(gata:dsRed)* double transgenic animals. Blood vessels are green fluorescent (I,K,L,N) and erythrocytes are red fluorescent (J,K,M,N). Extravasated erythocytes are clearly evident in the *gdf6a*^{s327} mutant (arrow in M). (**O,P**) Transmitted light images showing lateral views of the trunk of 2 dpf control (O) or *gdf6a* (P) morpholino-injected animals, showing normal overall morphology but trunk hemorrhage (asterisks) in the *gdf6a* morphants. 149/149 or 100% of control morpholino-

injected animals show no trunk hemorrhage, while 32/134 or 24% of *gdf6a* morpholino-injected animals show trunk hemorrhage, in 3 separate experiments. (**Q–V**) Representative transmitted light (Q,T), green confocal *Tg(kdrl:gfp)* (R,U), and red confocal Qdot655 nanocrystal (S,V) images of 2 dpf wild type sibling (Q–S) or *gdf6a*^{s327} mutant (T–V) *Tg(kdrl:gfp)* transgenic animals injected intravascularly with Qdot655 nanocrystals. Extensive Qdot655 leakage from vessels is evident in the *gdf6a*^{s327} mutant (arrows in V). (**W**) Quantification of the percentage of 2 dpf wild type sibling (0/11 in two separate experiments, 0%) or *gdf6a*^{s327} mutant animals (8/11 in two separate experiments, 73%) displaying leakage of Qdot655 nanocrystals injected into the circulation. (**X**) Quantification of the percentage of 2 dpf *hsp:mCherry*-injected (12/39 in two separate experiments, 31%;) or *hsp:gdf6a-2a-mCherry*-injected (11/142 in two separate experiments, 8%) *gdf6a*^{s327} mutant animals, heat shocked from 1 dpf, that display trunk hemorrhage. Expression of wild type *gdf6a* suppresses the *gdf6a*^{s327} mutant phenotype. All images are lateral views, rostral to the left. Scale bars are 70 μm in panels B, C, G–L, and P–U, 100 μm in panels M and N, and 1 mm in panels D and E.

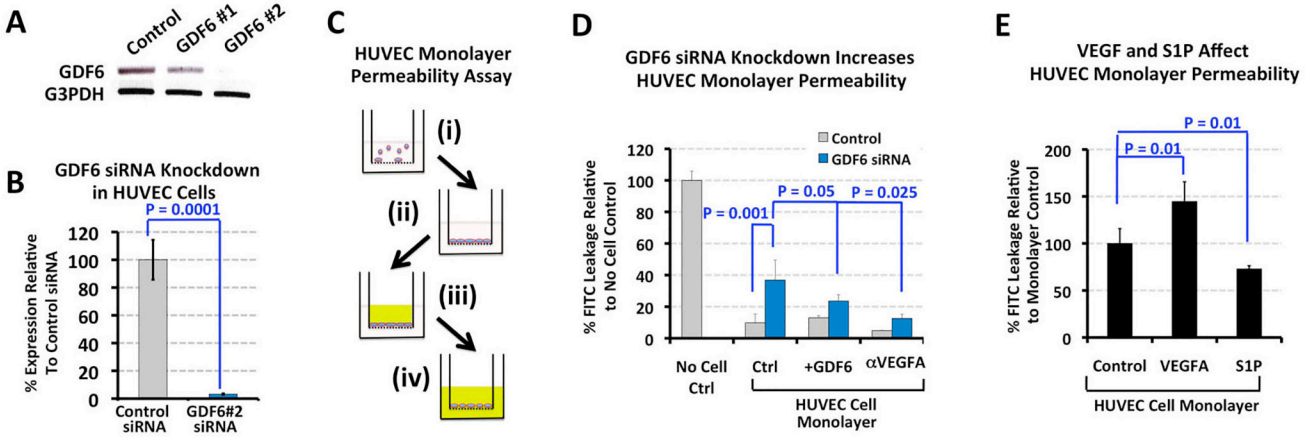

Figure 2. Loss of GDF6 function results in impaired vascular integrity *in vitro*

(**A**) RT-PCR of GDF6 and glyceraldehyde-3-phosphate dehydrogenase (G3PDH; loading control) from Human Umbilical Vein Endothelial Cell (HUVECs) that were treated with either control siRNA ("Control," column 1) or one of two different siRNAs targeting GDF6 ("GDF6 #1" and "GDF6 #2," columns 2 and 3). Both GDF6-targeting siRNAs knocked down GDF6 transcript levels, but siRNA #2 was much more effective. Observation noted from 3 independent experiments. (**B**) TaqMan assay quantitation of GDF6 transcript levels in control or GDF6 siRNA-treated HUVEC cells (both siRNAs were used in tandem to ensure maximal gene suppression efficiency for all experiments), showing greater than 90% reduction in GDF6 transcript levels in GDF6 siRNA-treated HUVEC. (**C**) Schematic diagram illustrating the HUVEC monolayer permeability assay. Briefly, HUVECs are seeded in the inner well of a transwell chamber in complete growth medium (i). The cells attach to the membrane and form cell-cell adhesions, assembling a confluent monolayer on the membrane prior to dye addition (ii). FITC-Dextran is added to the inner well of the transwell chamber, remaining largely contained within the inner chamber when cell-cell adhesion is intact (iii). Defects in endothelial cell-cell adhesion result in increased permeability across the monolayer and increased FITC-Dextran leakage into the outer, plate well. The intensity of fluorescence in the outer well is proportional to the extent of monolayer permeability (iv). (**D**) Quantification of the amount of FITC transferred through a HUVEC monolayer, expressed as a percentage of the amount of dye that transfers across the membrane in the absence of any added HUVEC cells (ie, no cell control). A control siRNA treated HUVEC monolayer reduces FITC transfer to approximately 10% of the no cell condition, but treating HUVEC with GDF6 siRNA results in a 3.5-fold increase in permeability. Treatment with either soluble GDF6 protein or anti-VEGFA antibody reduces the increased permeability caused by GDF6 siRNA knockdown. Equivalent results noted in 3 separate experiments. (**E**) Quantification of the amount of FITC transferred through the HUVEC monolayer, expressed as a percentage of the amount of dye that transfers across the membrane with a control HUVEC monolayer. VEGFA treatment results in increased monolayer permeability, while S1P treatment results in decreased monolayer permeability. qPCR data (panel B) was collected from at least 3 biological repeats with 3 technical repeats per probe. Permeability assays (panels D and E) were done as 3 biological replicates with at

least 3 technical repeats per each experimental condition. Data is shown from a single biological replicate.

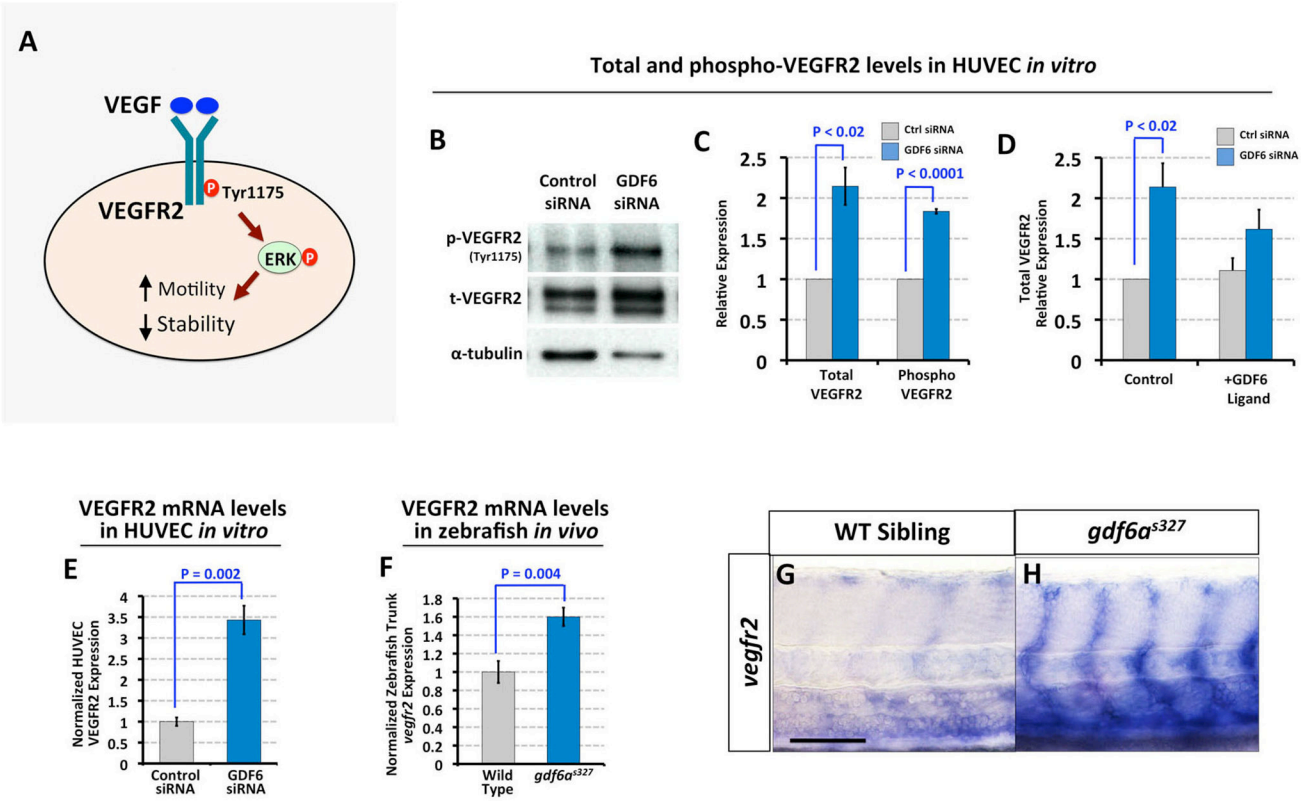

Figure 3. Loss of GDF6 function results in increased VEGFR2

(**A**) Schematic diagram showing that VEGF activation leads to phosphorylation of tyrosine 1175 on the VEGFR2 receptor, leading to activation (phosphorylation) of ERK, which in turn promotes increased endothelial cell motility and proliferation. (**B**) Representative images of western blots used to measure levels of phospho (Tyr 1175) VEGFR2 or total VEGFR2 protein versus an a-tubulin loading control, using extracts from ether control siRNA- or GDF6 siRNA-treated HUVEC *in vitro*. (**C**) Quantification of phospho (Tyr 1175) VEGFR2 and total VEGFR2 protein levels normalized to a-tubulin loading controls, using extracts from either control siRNA- or GDF6 siRNA-treated HUVEC *in vitro*. Protein levels are expressed as percentages of control siRNA-treated amounts. (**D**) Quantification of total VEGFR2 protein levels in control siRNA- or GDF6 siRNA-treated HUVEC treated with either nothing or with recombinant GDF6 protein, normalized to a-tubulin loading controls. Protein levels are expressed as percentages of control siRNA-treated amounts. (**E**) TaqMan assay quantitation of VEGFR2 transcript levels in control or GDF6 siRNA-treated HUVEC cells, showing an approximate 3.5-fold increase in VEGFR2 transcript levels in GDF6 siRNA-treated HUVEC. (**F**) TaqMan assay quantitation of VEGFR2 transcript levels in the trunks of 36 hpf wild type sibling or *gdf6a*^{s327} mutant animals, showing a 1.6-fold increase in *vegfr2* transcript levels. (**G,H**) Whole mount *in situ* hybridization of the mid-trunk of 36 dpf wild-type sibling (G) and *gdf6a*^{s327} mutant (H) animals probed for *vegfr2*, showing increased vascular expression. Images are lateral views, rostral to the left. Scale bar = 50 μm. Western blot results are shown from 2–3 independent biological repeats. Protein lysates from each biological repeat were blotted twice for each antibody (two technical repeats). qPCR data was collected from at least 3 biological repeats with 3 technical repeats per probe. WM-

ISH was performed in 3 biological replicates with at least 10 embryos per experimental group.

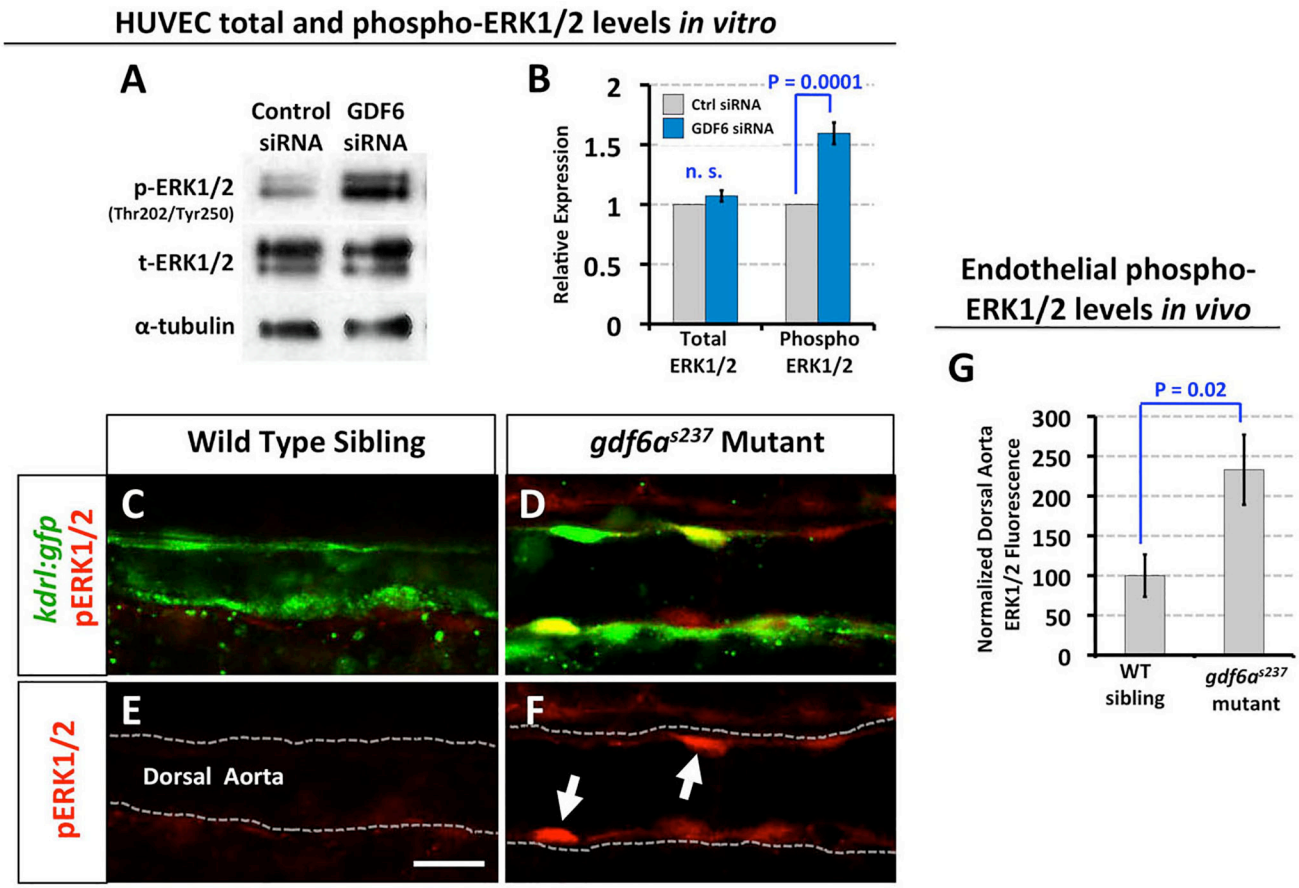

Figure 4. Loss of GDF6 function results in increased ERK activation

(**A**) Representative images of western blots used to measure levels of phospho-ERK1/2 (Thr 202, Tyr 205) or total ERK1/2 protein versus an alpha-tubulin loading control, using extracts from ether control siRNA- or GDF6 siRNA-treated HUVEC *in vitro*. (**B**) Quantification of phospho-ERK1/2 (Thr 202, Tyr 205) and total ERK1/2 protein levels normalized to alpha-tubulin loading controls, using extracts from either control siRNA- or GDF6 siRNA-treated HUVEC *in vitro*. Protein levels are expressed as percentages of control siRNA-treated amounts. (**C–F**) Representative confocal images of the dorsal aorta in a 2 dpf wild type sibling (C,D) or *gdf6a*^{s327} mutant (E,F) *Tg(kdrl:gfp)* transgenic zebrafish (green; panels C,D) subjected to immunostaining with phospho-ERK1/2 (Thr 202, Tyr 205) antibody. (red; panels C–F). (**G**) Quantification of phospho-ERK1/2 axial vessel fluorescence intensity in 2 dpf *Tg(kdrl:gfp)* transgenic zebrafish subjected to immunostaining with phospho-ERK1/2 (Thr 202, Tyr 205) antibody. Images are lateral views, rostral to the left. Scale bar is 5 μm. Western blot results are shown from at least 3 independent biological repeats. Protein lysates from each biological repeat were blotted twice for each antibody (two technical repeats). IHC for p-Erk1/2 was performed in 3 biological replicates with at least ten embryos per experimental group.

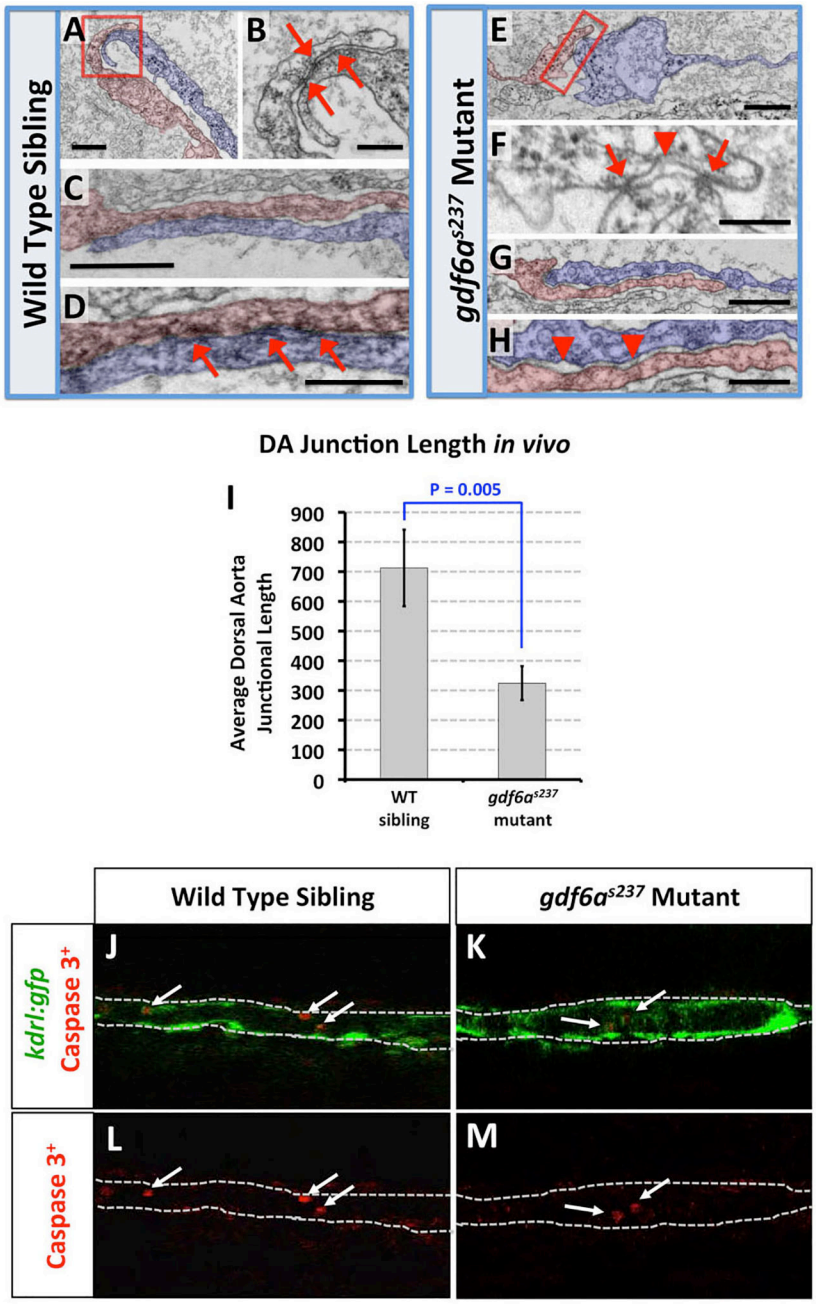

Figure 5. Loss of GDF6 function results in defects in endothelial cell-cell junction formation but not increased cell death

(**A–D**) Transmission electron micrographs of dorsal aorta endothelial cells in wild type sibling animals. Images show junctional interfaces between two different endothelial cells in the wall of the dorsal aorta (pseudocolored in blue and red in panels A,C, and D). Panel B shows a magnified image of the boxed region in panel A, while panel D shows a magnified image of the endothelial cell-cell interface in panel C. Wild type endothelial cell membranes are closely apposed at their cell-cell interfaces, with abundant readily apparent electron-dense junctional complexes (red arrows in panels B and D). (**E–H**) Transmission electron micrographs of dorsal aorta endothelial cells in *gdf6a*^{s327} mutant animals. Images show

junctional interfaces between two different endothelial cells in the wall of the dorsal aorta (highlighted in blue and red in panels E,G, and H). Panel F shows a magnified image of the boxed region in panel E, while panel H shows a magnified image of the endothelial cell-cell interface in panel G. Mutant endothelial cell membranes often appear less closely apposed to one another than observed at endothelial cell interfaces in wild type siblings (red arrowheads in panels F and H), with fewer electron-dense junctional complexes (red arrows in panel F). (**I**) Quantification of the average length of endothelial cell-cell junctions measured from transmission electron micrographs of dorsal aorta endothelial cells in wild type sibling or *gdf6a*^{s327} mutant animals. All transmission electron micrographs are from transverse sections of the trunk (and dorsal aorta). Scale bars are 500 nm in panels A,C,E,G and 250 nm in panels B,D,F,H. Images of dorsal aortae from 5 wild type and 10 mutant embryos were used for morphometry to determine morphological characteristics of the junctions. (**J–M**) Confocal images of the dorsal aorta in 2 dpf *Tg(kdrl:egfp)* transgenic wild type sibling (J,L) or *gdf6a*^{s327} mutant (K,M) caspase 3 immunostained animals, showing *egfp* (green) and caspase 3 (red) staining (J,K) or caspase 3 staining alone (red; L,M). Arrows point to caspase 3 positive cells. White dotted lines indicate the boundaries of the aorta. At least 5 wild type and mutant embryos in 2 independent experiments were immunostained and imaged for analysis, showing consistent results.

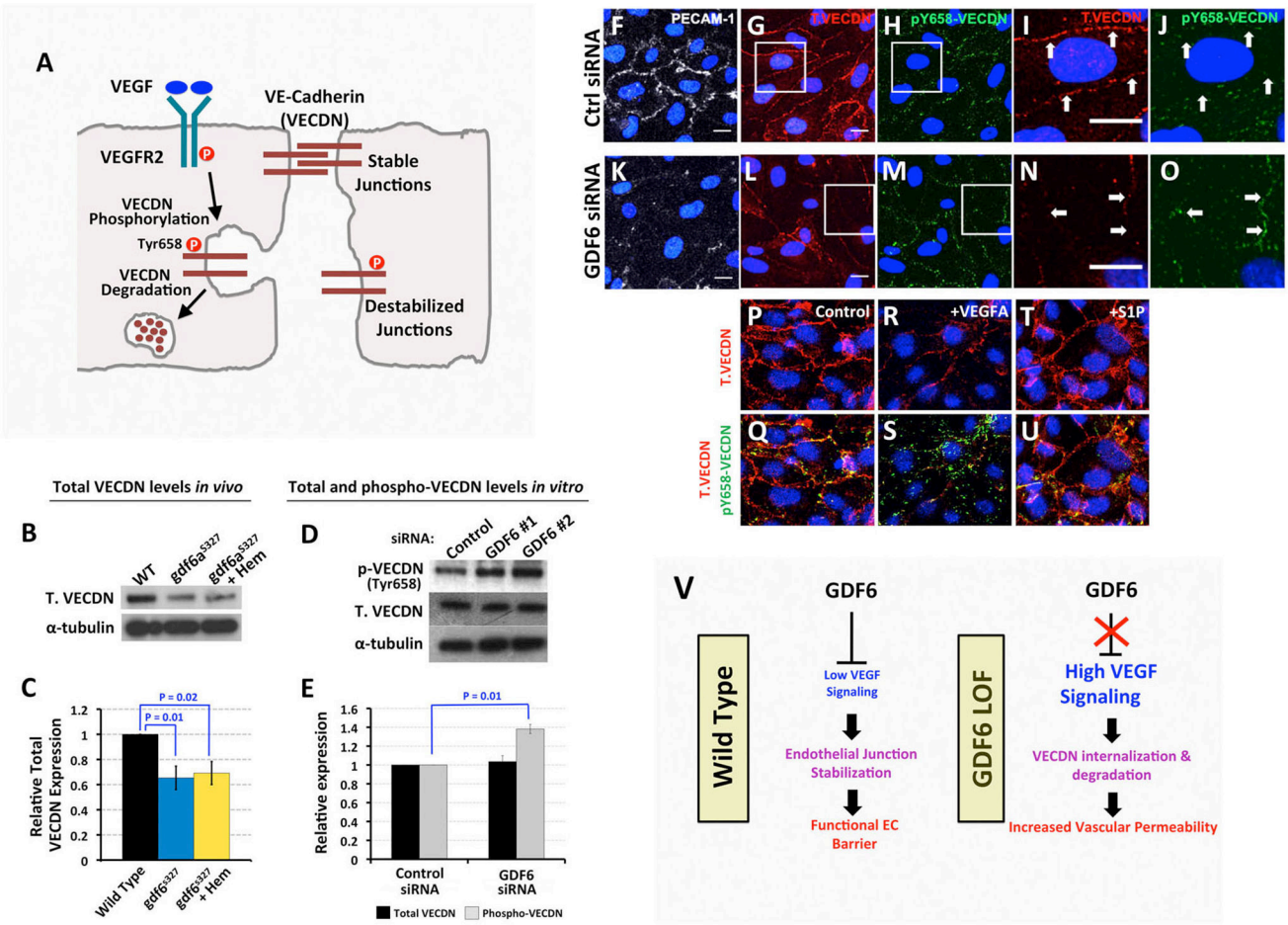

Figure 6. Loss of GDF6 function results in VE-Cadherin destabilization

(**A**) Schematic diagram showing that VEGF activation results in phosphorylation of tyrosine 658 (Y658) on VE-Cadherin (VECDN), which leads to VECDN internalization and degradation. (**B**) Representative images of western blots used to measure levels of total VECDN protein versus an a-tubulin loading control, using protein extracts from wild type siblings, non-hemorrhaging *gdf6a*^{s327} mutants, or *gdf6a*^{s327} mutants with trunk hemorrhage. (**C**) Quantification of total VECDN protein levels normalized to a-tubulin loading controls, using protein extracts from wild type siblings, non-hemorrhaging *gdf6a*^{s327} mutants, or *gdf6a*^{s327} mutants with trunk hemorrhage. (**D**) Representative images of western blots used to measure levels of phospho-VECDN (Y658) or total VECDN protein versus an a-tubulin loading control, using protein extracts from HUVEC cells treated with either control siRNA or one of two different GDF6 siRNAs. (**E**) Quantification of phospho-VECDN (Y658) or total VECDN protein levels normalized to an a-tubulin loading control, using protein extracts from HUVEC cells treated with either control siRNA or one of two different GDF6 siRNAs. Protein levels are expressed as fractions of control siRNA-treated amounts. (**F–O**) Representative confocal images of control (F–J) or GDF6 (K–O) siRNA-treated HUVECs in endothelial monolayers, subjected to immunofluorescence staining using antibodies against PECAM (grey-F,K), total VECDN (red-G,I,L,N), and phospho-VECDN (Y658) (green-H,J,M,O). Panels H,J,M,O are magnified views of the boxed regions in panels G,I,L,N,

respectively. PECAM and VECDN images show reduced cell-cell junctional staining in GDF6 siRNA treated HUVEC, but strong phospho-VECDN (Y658) staining of some of the remaining junctions. (**P–U**) Representative confocal images of control HUVECs in endothelial monolayers, treated with nothing (P,Q), VEGFA recombinant protein (R,S), or S1P (T,U) overnight then subjected to immunofluorescence staining using antibodies against total VECDN (red, P–U), and phospho-VECDN (Y658) (green, Q,S,U). Merged images of phospho-VECDN (Y658) and total VECDN (Q,S,U) show their relative localization patterns. Western blot results are shown from at least 2 independent biological repeats. Protein lysates from each biological repeat were blotted twice for each antibody (two technical repeats). Immuostaining assays were done as at least 2 biological replicates with a minimum or 2 technical replicates per each experimental condition, and 5 images analyzed per replicate. (**V**) Model for the role of GDF6 in endothelial barrier formation. GDF6 activity restrains VEGF activity, promoting endothelial junction stabilization. GDF6 loss-of-function (LOF) results in increased VEGF signaling, increased VECDN phosphorylation, internalization, and degradation, and reduced endothelial barrier function.